doi.org/10.26434/chemrxiv.11089097.v1

On the Bonding Situation in Stannocene and Plumbocene N-Heterocyclic Carbene Complexes

Diego Andrada, Sergi Danés, Lisa Wirtz, Carsten Mueller, Volker Huch, Theresa Block, Rainer Pöttgen, André Schäfer

Submitted date: 24/11/2019 • Posted date: 29/11/2019

Citation information: Andrada, Diego; Danés, Sergi; Wirtz, Lisa; Mueller, Carsten; Huch, Volker; Block, Theresa; et al. (2019): On the Bonding Situation in Stannocene and Plumbocene N-Heterocyclic Carbene Complexes. ChemRxiv. Preprint. https://doi.org/10.26434/chemrxiv.11089097.v1

A detailed experimental and computational study of a series of stannocene and plumbocene N-heterocyclic carbene complexes is presented. This unique class of group 14 Lewis acid base adducts was obtained from reactions of the corresponding metallocenes and N-heterocyclic carbenes (NHC), and were structurally characterized by single crystal X-ray diffraction. The obtained structures show a perpendicular pose of the NHC with respect to the metallocene, hence precluding the maximal interaction between the moieties. The nature of the Sn-CNHC and Pb-CNHC bonds have been investigated by applying Energy Decomposition Analysis (EDA-NOCV). For the sake of comparison, known stannocene and plumbocene Lewis base complexes have been included in the series. The attractive chemical bonding interactions are around 50% electrostatic, 30% covalent and 20% dispersion. Indeed, dispersion interactions play a determining role the bigger the substituents become. The covalent interactions derive from the donation of the carbene ligand into the empty p orbital of the metallocene.

On the Bonding Situation in Stannocene and Plumbocene *N*-Heterocyclic Carbene Complexes

Sergi Danés[†§], Carsten Müller[†§], Lisa Wirtz[†§], Volker Huch[†], Theresa Block[‡], Rainer Pöttgen[‡*], André Schäfer[†*], and Diego M. Andrada[†*]

[†]Saarland University, Faculty of Natural Sciences and Technology, Department of Chemistry, Campus Saarbrücken, 66123 Saarbrücken, Federal Republic of Germany

[‡] University of Münster, Faculty of Chemistry and Pharmacy, Institute of Inorganic and Analytical Chemistry, Corrensstrasse 30, 48149 Münster, Federal Republic of Germany

ABSTRACT: A detailed experimental and computational study of a series of stannocene and plumbocene *N*-heterocyclic carbene complexes is presented. This unique class of group 14 Lewis acid base adducts was obtained from reactions of the corresponding metallocenes and *N*-heterocyclic carbenes (NHC), and were structurally characterized by single crystal X-ray diffraction. The obtained structures show a perpendicular pose of the NHC with respect to the metallocene, hence precluding the maximal interaction between the moieties. The nature of the Sn-C^{NHC} and Pb-C^{NHC} bonds have been investigated by applying Energy Decomposition Analysis (EDA-NOCV). For the sake of comparison, known stannocene and plumbocene Lewis base complexes have been included in the series. The attractive chemical bonding interactions are around 50% electrostatic, 30% covalent and 20% dispersion. Indeed, dispersion interactions play a determining role the bigger the substituents become. The covalent interactions derive from the donation of the carbene ligand into the empty *p* orbital of the metallocene.

INTRODUCTION

Since the first isolation and structural characterization of a persistent, "bottleable", *N*-heterocyclic carbene (NHC) by Arduengo and coworkers,[1] following the pioneering work of Wanzlick,[2] these compounds have become one of the most important class of ligands throughout main group and transition metal chemistry.[3, 4] In main group chemistry, numerous examples of NHC Lewis acid adducts have been reported. Particularly, in low-valent p block chemistry, they have seen wide application as strong σ donor ligands, stabilizing and enabling isolation of compounds, otherwise unstable and non-isolable in the condensed phase. Among others, a well-recognized and particularly important class of such compounds are heavy tetrylene-NHC complexes of the type NHC•ER_2 (E = Si, Ge, Sn, Pb), which are known for various halo- and organo-substituted heavy tetrylenes.[5-8]

CHART 1. Different stannocene and plumbocene Lewis base complexes.

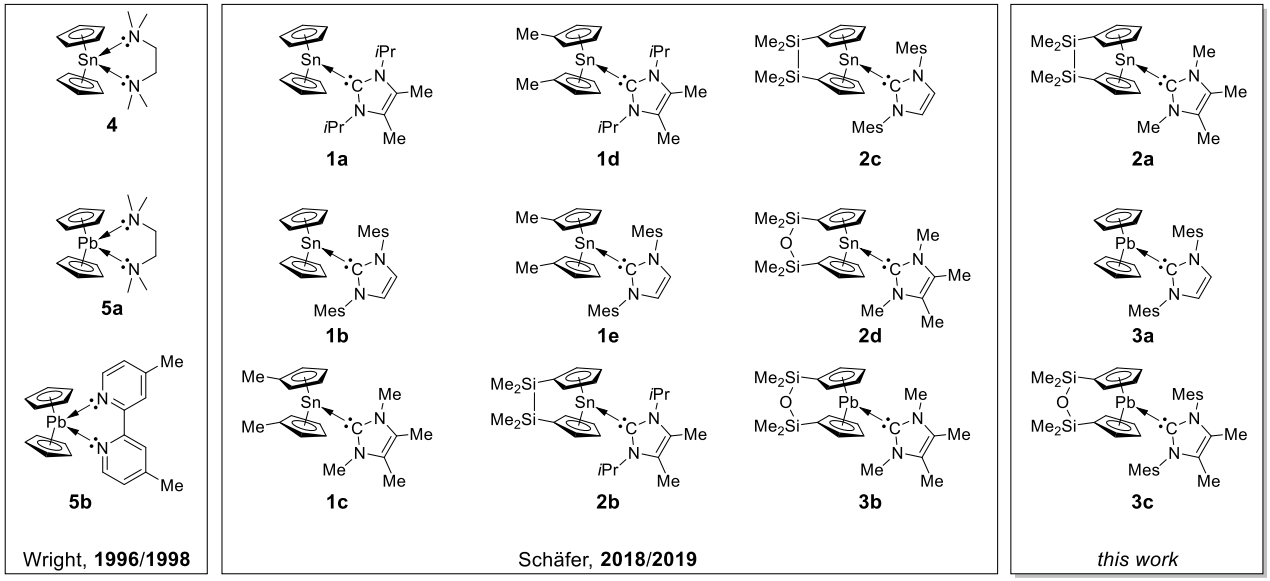

Surprisingly, the reactivity of the longest known diorganotetrylene-type compounds, stannocene, and plumbocene, towards NHCs is almost unexplored.[9] This might be because these metallocenes are often not regarded as "true" tetrylenes, since they lack any strong σ donor abilities, but rather exclusively exhibit Lewis acidic character. While complexes of plumbocene and stannocene with nitrogen bases are known since the 1990s and NHC complexes of group 2 and group 4 metallocenes have also been described, the first isolation and structural characterization of group 14 metallocene (tetrelocene) NHC complexes has only recently been reported by the Schäfer group (Chart 1).[10-12] It was recognized early on that these complexes show much higher reactivity than their reactants, resulting in low thermal stability, requiring isolation and characterization at low temperatures in some cases. Furthermore, these complexes all exhibit unusually long metal-carbon bonds and the complexation energy of the NHC to the metallocene is rather small. Consequently, these complexes exist in a dissociative equilibrium in solution at room temperature. In the present study, we give a thorough analysis and description of the chemical bonding nature in these species, using *ab initio* and DFT methods. The E-C^{NHC} and E-N interactions have been analyzed with Energy Decomposition Analysis (EDA) in combination with the Natural Orbitals for Chemical Valence (NOCV).

RESULTS AND DISCUSSION

Treatment of a corresponding stannocene or plumbocene with a suitable NHC results in the formation of the corresponding adduct (Scheme 1).

SCHEME 1. Synthesis of stannocene and plumbocene N-heterocyclic carbene complexes, 1a-e, 2a-d, 3a-c.

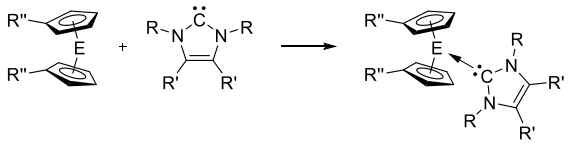

1a-e, **2a-d**, **3a-c**

1a: E = Sn, R = *i*Pr, R' = Me, R'' = H; **1b**: E = Sn, R = Mes, R' = H, R'' = H; **1c**: E = Sn, R = Me, R' = Me, R'' = Me; **1d**: E = Sn, R = *i*Pr, R' = Me, R'' = Me; **1e**: E = Sn, R = Mes, R' = H, R'' = Me; **2a**: E = Sn, R = Me, R' = Me, R'' = μ-Si_2Me_4; **2b**: E = Sn, R = *i*Pr, R' = Me, R'' = μ-Si_2Me_4; **2c**: E = Sn, R = Mes, R' = H, R'' = μ-Si_2Me_4; **2d**: E = Sn, R = Me, R' = Me, R'' = μ-Si_2Me_4O; **3a**: E = Pb, R = Mes, R' = H, R'' = H; **3b**: E = Pb, R = Me, R' = Me, R'' = μ-Si_2Me_4O; **3c**: E = Pb, R = Mes, R' = H, R'' = μ-Si_2Me_4O.

As described earlier, the stannocene and plumbocene NHC complexes exist in a dissociative equilibrium in solution at room temperature, but can be isolated as crystalline solids at low temperatures. In addition to the already reported stannocene- and plumbocene-NHC complexes, **1a-e**, **2b-d**, **3b**,[9, 13] we were able to isolate and structurally characterize the 1,3,4,5-tetramethylimidazole-2-ylidene-stannocene adduct, **2a**, and, more significantly, 1,3-dimesitylimidazole-2-ylidene-plumbocene complexes **3a**,**c** (Figure 1). The latter represent rare examples of bis(cyclopentadienyl)lead(II) carbene complexes and allow for structural comparison to their previously reported tin analogues. Structural features of **2a** are similar to the other 1,3,4,5-tetramethylimidazole-2-ylidene stannocene adducts, **1c**, **2d**, reported previously.[9]

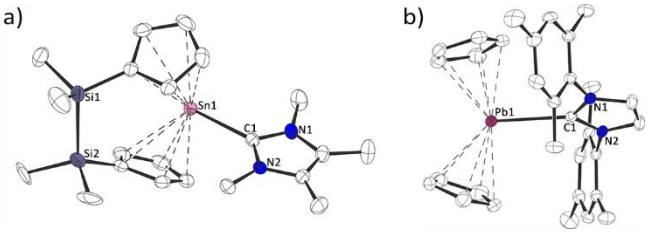

Figure 1. Molecular structure of a) stannocenophane-NHC complex **2a** and b) plumbocene-NHC complex **3a** in the crystal (displacement ellipsoids at 50% probability level, H-atoms omitted for clarity). Selected experimental bond lengths and angles: **2a**: Sn-C1: 237.6 pm, Sn-$Cp^{centroid}$: 260.5-266.3 pm, ∠Cp-Cp: 57.4°; **3a**: Pb-C1: 272.5 pm, Pb-$Cp^{centroid}$: 257.1-257.7 pm, ∠Cp-Cp: 41.7°.

Strikingly, in the plumbocene-NHC complex, **3a**, the coordination of the NHC to the lead atom is significantly different. In all reported stannocene-NHC complexes, as well as in previously reported plumbocene-NHC complex **3b**, a "side-on" coordination of the carbene is observed. This has been rationalized by the shape of the frontier molecular orbitals.[9] While the HOMO and HOMO-1 in tetrelocenes correspond to the π system of the cyclopentadienyl ligands, the LUMO exhibits a large coefficient at the central atom in the shape of a *p* orbital, perpendicular to the Cp-E-Cp plane. In addition, the energetically low lying lone pair spatial demand also contributes to this coordination mode (see *infra* Figure 5). In contrast, in the plumbocene-NHC complex **3a** with the N-mesityl-substituted NHC, a "face-on" coordination is observed which is counterintuitive on the first glance. A similar, yet less pronounced "face-on" arrangement of the NHC in complex **3c** is observed (Figure 2).

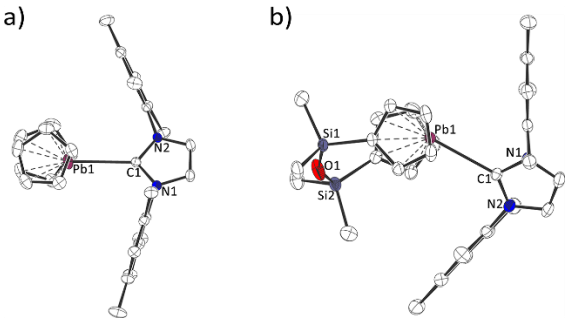

Figure 2. Molecular structure of a) plumbocene-NHC complex **3a**, b) plumbocenophane-NHC complex **3c** in the crystal (displacement ellipsoids at 50% probability level, H-atoms omitted for clarity).

Other structural features in **3a**,**c** are very long Pb-C^{NHC} bonds of 272.5 pm (**3a**) and 273.4 pm (**3c**), which, in case of **3a**, is 26 pm longer than in the tin analogue, **1b**. The Pb-$Cp^{centroid}$ distances in **3a**,**c** are elongated compared to the corresponding plumbocenes (257.1-257.7 pm in **3a** *vs* 244.1-252.7 pm in Cp_2Pb; 256.0/259.0 pm in **3c** *vs* 243.0/256.0 pm in μ-$Si_2Me_4O(C_5H_4)_2Pb$), while the C-C bonding distances within the Cp moieties remain relatively uniform, indicating a high degree of aromaticity.[14] The orientation of the NHC plane relative

to the Cp-Pb-Cp plane is 64° in **3a** and 58.4° in **3c**, which is significantly smaller than in all tin-NHC complexes (around 90°).

In order to unravel the bonding situation of compounds **1a-e**, **2a-d** and **3a-c** as well as **4** and **5a**,**b**,[15, 16] we performed quantum chemical calculations at the B3LYP+D3/def2-TZVP level of theory (Figure 3). In general, the calculated E-C^{NHC} bonds and Cp-E lengths are ca. 10 pm longer than those experimentally measured. This difference is usually observed in cyclopentadienyl complexes since their coordination strongly depends on the crystal structure environment (packing effects).[17] As stated before, the tetrelocene-NHC complexes exhibit very long Sn-C^{NHC} and Pb-C^{NHC} bonds. Thus, **2a** with the shortest Sn-C^{NHC} bond of this series is slightly longer than in other Sn^{II}-NHC complexes reported elsewhere, for instance, NHC-$SnCl_2$ (235.8 pm).[18, 19] The computed Sn-C^{NHC} bond lengths range 19.0 ppm, with complex **1c** being the one with shorter distance (250.1 ppm) and **1e** (269.1 ppm) the one exhibiting the longest distance of the here studied series.

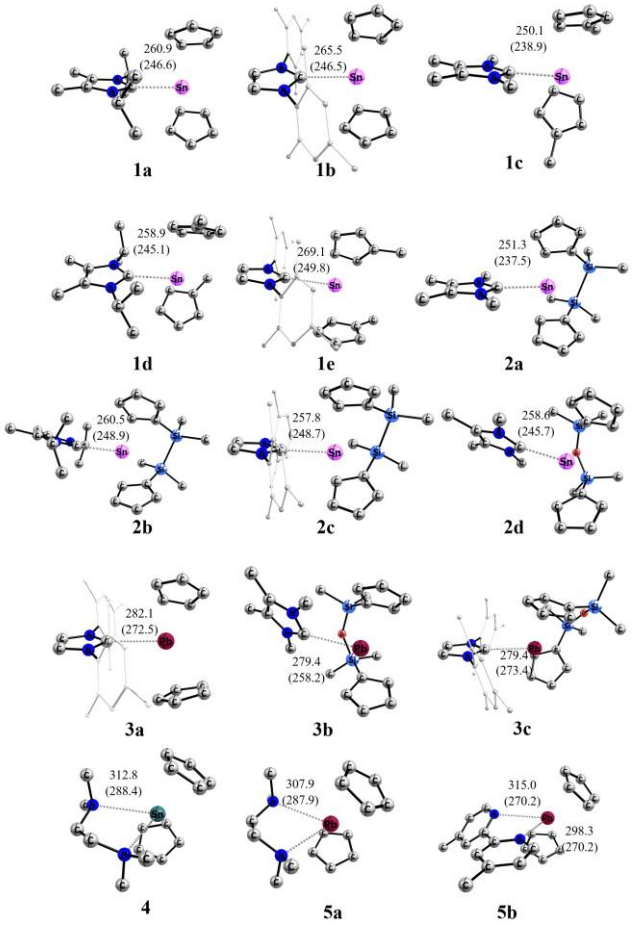

Figure 3. Calculated geometries of complexes **1**-**5** with selected bond length (in pm) at B3LYP+D3/def2-TZVP (experimental values in parenthesis);[9, 15, 16] Hydrogen atoms omitted for clarity.

All in all the Sn-C^{NHC} and Pb-C^{NHC} bonds found in these metallocene-NHC complexes are along the longest ever structurally characterized two-center-two-electron Sn-C and Pb-C bonds. As to be expected, the volume of the substituents on the nitrogen atom of the NHC influences the E-C^{NHC} bond distances. In case of the stannocene complexes, when R = Me the bond is shorter while for R = Mes the bonds are longer. The nature of the *ansa*-bridge on some of the tetrelocenophanes does not have strong influence on the bond distances. The direct comparison of the lead derivatives **3a-c** reveals that the effect of the substituent on the nitrogen atoms of the NHC holds true, although there are only three examples, **3a-c**, with two different NHCs, the Pb-C^{NHC} bond in **3b** is significantly shorter (258.4.4 pm) than in **3a** (272.4 pm) and **3c** (273.4 pm). Noteworthy, plumbocene-NHC complex **3a** displays a different complexation mode, as it is apparently more flexible regarding the complexation place of the carbene ligand, than the corresponding stannocene complexes. While all the stannocene complexes, **1a-e**, **2a-d**, display exclusively a "side-on" complexation of the NHC ligand, the lead analogues **3a** shows a "face-on" coordination, while **3b** exhibits a side-on coordinated NHC ligand as well and **3c** is somewhat in between these two. This is a consequence of many factors such as weak Pb-C^{NHC} bonds, more room on the metal of the metallocene due to longer metal-Cp bonds in case of lead than in case of tin, and lower hybridization of the Pb atom than of the Sn atom.

We analyzed the electronic structure of **1-5** by NBO analysis. Table 1 gathers the calculated partial charges and Wiberg bond orders of the E-C^{NHC} and E-N^{ligand} (E = Sn, Pb) bonds. The weakness of the bonding of the carbene ligands to the Sn and Pb atoms is reflected by the Wiberg Bond order values (P). The bond orders for complexes **1**-**3** range from 0.3 to 0.4 a.u., being the highest P for the smallest ligands, in good agreement with the shorter bond lengths.

Table 1. NBO results for 1-5 at B3LYP+D3/def2-TZVP level of theory: Wiberg bond order (P), hybridization, and partial charges (q).

	Q(E)	Q(C^{carb}/N)	Q(ECp_2)	P(E-C^{carb}/N)	Hyd (E)
1a	**1.04**	**0.12**	**-0.21**	**0.35**	***s*(94.5%)** ***p*(5.5%)**
1b	**1.11**	**0.13**	**-0.18**	**0.31**	***s*(94.9%)** ***p*(5.1%)**
1c	**0.98**	**0.13**	**-0.24**	**0.42**	**s(90.7%)** ***p*(9.3%)**
1d	**1.06**	**0.11**	**-0.21**	**0.36**	**s(94.1%)** ***p*(5.9%)**
1e	**1.13**	**0.13**	**-0.17**	**0.30**	**s(96.1%)** ***p*(3.9%)**
2a	**1.16**	**0.10**	**-0.18**	**0.32**	**s(94.3%)** ***p*(5.7%)**
2b	**1.08**	**0.09**	**-0.21**	**0.34**	**s(95.1%)** ***p*(4.9%)**
2c	**1.02**	**0.11**	**-0.34**	**0.41**	**s(91.7%)** ***p*(8.2%)**
2d	**1.06**	**1.10**	**-0.22**	**0.37**	**s(93.4%)** ***p*(6.6%)**
3a	**1.15**	**0.12**	**-0.15**	**0.25**	**s(99.4%)** ***p*(0.6%)**
3b	**1.16**	**0.09**	**-0.18**	**0.30**	**s(98.2%)** ***p*(1.8%)**
3c	**1.21**	**0.11**	**-0.15**	**0.24**	**s(99.1%)** ***p*(0.9 %)**
4	**1.19**	**-0.42**	**-0.10**	**0.06**	**s(99.9%)** ***p*(0.1%)**
5a	**1.23**	**-0.43**	**-0.11**	**0.06**	**s(100.0%)** ***p*(0.0%)**
5b	**1.19**	**-0.43/-0.42**	**-0.08**	**0.08/0.06**	**s(99.8%)** ***p*(0.2%)**

Examination of the overall charge distribution by Natural Partial Atomic (NPA) charges reveal that the ligands are donating to the metallocene moiety around 0.2 e. For the plumbocene complexes, the NPA values are slightly lower: 0.15 e for **3a** 0.18 e for **3b**. The NBO orbitals (Figure 4; Figures S3-S16) show a lone pair on the carbene carbon atom and a lone pair on the metal center. For some complexes, NBO localized E-C^{NHC} single bonds which are strongly polarized towards the carbene carbon atom are observed. The selection of a donor-acceptor representation leads to a non-Lewis occupancy of 2.1% compared to the 1.9% for the former representation (Table S2). The lone pairs on the Sn and Pb atoms are mostly *s* hybridized, which counts 90 to 95% for Sn, and 98 to 100% for Pb. These hybridization differences might be one of the main reasons for the counterintuitive face-on complexation that is observed in case of **3a**,**c** since there is no directional Pauli repulsion. Second-order perturbation theory within the NBO framework suggest a two-electron stabilization of the carbene lone pair into the vacant *p* orbital of Sn and Pb. Our calculations estimate values of around -35 to -46 kcal mol^{-1} for E = Sn and, -35 kcal mol^{-1} for E = Pb. The stronger interaction for Sn than Pb goes in line with the computed occupancy. Thus, tin exhibits higher *p* occupancy (0.41 e) than lead (0.31 e). Note that **1c** has the strongest stabilization interaction (62 kcal mol^{-1}) in line with the shortest bond (250.1 pm) of the series.

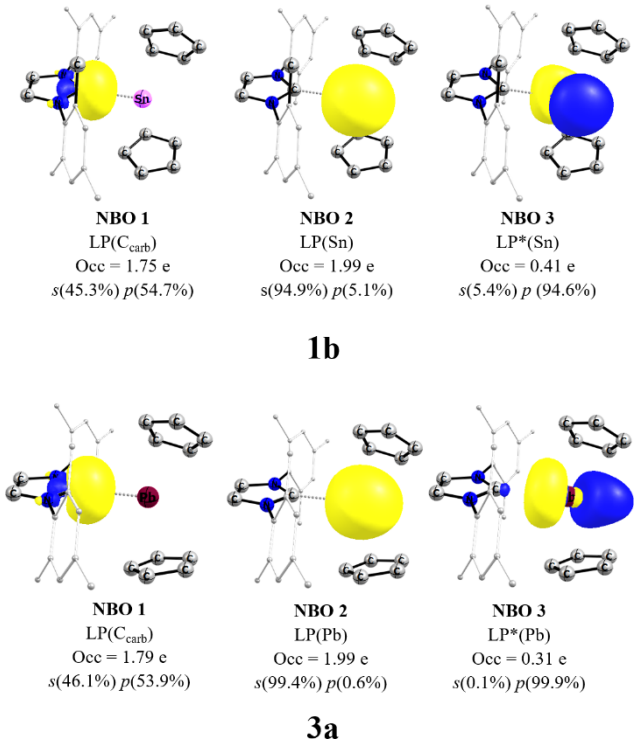

Figure 4. Selected NBO orbitals of compounds **1b** and **3a** at the B3LYP+D3/def2-TZVP level of theory. Hydrogen atoms were omitted for clarity.

To examine the strength of the E-C^{NHC} (E= Sn, Pb)) bonds in NHC complexes **1a-e**, **2a-d**, **3a-c**, we have computed and compared the dissociation energies of this complex series. Table 2 gives the bond energies at the BP86+D3(BJ)/ZORA&TZ2P level of theory using the optimized structures. The computed bond dissociation energies (D_e in Table 2) suggest a small change on the strength of the bond for the different complexes. Despite the small difference, stannocene complexes show a clear trend, which depends on the size of the carbene substituents. Remarkably, opposite to the observation of the bond distances, sterically less demanding carbenes with smaller substituents on the nitrogen atoms exhibit weaker bonds (e.g. **1c**: -16.7 kcal mol^{-1}), whereas sterically more demanding carbenes carrying larger groups on the nitrogen atoms are more strongly bonded (e.g. **2c**: -27.9 kcal mol^{-1}). This goes in line with experimental observations that **1c** is only marginally stable at room temperature and decomposes within minutes to hours in solution, while **2c** is stable at ambient conditions for longer periods.[9] Lead complexes show stronger bonded NHC ligands than the tin complexes regardless the bond distances are longer. Thus, the bond length does not directly correlate with the bond-strength. This fact has previously been observed for other Lewis pairs.[20, 21] Indeed, this result hints at the relative importance of the dispersion interactions in order to stabilize these metallocene complexes, explaining, for instance, the carbene position in compound **3b**. It has been demonstrated by Schreiner *et al.*[22] and Power *et al.*[23] that bulky groups do not only provide kinetic stability but also thermodynamic stability by their attractive interactions. Further dissection has been performed by Energy Decomposition Analysis (EDA),[24-26] for a more in-depth understanding of the interactions between the metallocenes and the ligand molecules. EDA has proven to be a powerful tool for improving the understanding of chemical bonding in main-group compounds and transition metal compounds.[6, 27-29] Within this method the bond formation between two or more interacting fragments is divided in three steps (see Computational Details). In the first step, the fragments, which are calculated using the frozen geometries within the entire molecule, are placed into the molecule disposition without electronic relaxation to yield the electrostatic interaction (ΔE_{elstat}). In the second step, the wave function is antisymmetrized and renormalized giving the Pauli repulsion within the fragments (ΔE_{Pauli}). In the third step, the molecular orbitals relax into the final state to yield the stabilizing orbital term (ΔE_{orb}). Also, the stabilizing dispersion interaction can be computed (ΔE_{disp}). The sum of all the terms gives the total interaction energy ΔE_{int}. The dissociation energy can be calculated by combining the interaction energy together with the preparation energy (ΔE_{prep}), which is the energy needed to promote the fragments from their equilibrium geometry to the geometry and electronic state in the compounds.

As the first approach, we have performed EDA calculations selecting the fragments Cp_2E (E = Sn, Pb) and the different carbenes. The numerical results are presented in Table 2. The interaction energy between the two fragments ranges from -30.1 to -42.3 kcal mol^{-1}. The bond dissociation energy (D_e) of stannocenes follows the same trend since the preparation energy only involves the deformation of the σ-donating ligand and the metallocene moieties. The total preparation energies are around 10 kcal mol^{-1}, which accounts for the deformation of the stannocene to give room to the interacting carbene. The fact that the plumbocene NHC complexes exhibit stronger bonded NHC ligands than the tin analogues is a consequence of a lower preparation energy penalty, which is only 5 kcal mol^{-1} since the potential energy surface of Cp_2Pb is more shallow than that of Cp_2Sn. Further partition of the interaction term shows that the Pauli repulsion in stannocene complexes is stronger than in plumbocene complexes, in line with the shorter bond length.

Table 2. Energy decomposition analysis (EDA-NOCV) of the E-C^{NHC} bonds (E =Sn, Pb) in compounds 1-3 at BP86+D3(BJ)/ZORA&TZ2P level of theory. Energy values are given in kcal mol^{-1}.

	1a	1b	1c	1d	1e	2a	2b	2c	2d	3a	3b	3c
ΔE_{int}	-30.5	-35.8	-30.1	-31.1	-33.2	-30.2	-33.7	-42.3	-31.7	-32.9	-29.6	-36.5
ΔE_{Pauli}	87.5	72.6	99.4	92.4	69.0	95.9	87.2	88.3	89.5	55.4	58.9	60.2
ΔE_{elstat}[a]	-62.2 (52.7%)	-52.0 (48.0%)	-74.6 (57.6%)	-65.1 (52.7%)	-48.0 (46.9%)	-72.4 (57.5%)	-62.5 (51.7%)	-63.3 (48.5%)	-65.8 (54.3%)	-40.9 (46.3%)	-44.7 (50.5%)	-43.9 (45.4%)
ΔE_{disp}[a]	-16.5 (13.9%)	-22.3 (20.6%)	-11.0 (8.5%)	-17.4 (14.1%)	-22.5 (22.0%)	-10.8 (8.6%)	-17.9 (14.8%)	-25.4 (19.4%)	-15.3 (12.6%)	-23.1 (26.1%)	-17.2 (19.5%)	-26.2 (27.1%)
ΔE_{orb}[a]	-39.3 (33.3%)	-34.0 (31.4%)	-43.9 (33.9%)	-41.1 (33.2%)	-31.8 (31.1%)	-42.9 (34.0%)	-40.5 (33.5%)	-41.9 (32.1%)	-40.1 (33.1%)	-24.3 (27.5%)	-26.6 (30.1%)	-26.6 (27.5%)
$\Delta E_{orb\ \sigma\text{-}don}$[b]	-29.4 (74.6%)	-24.6 (72.3%)	-34.8 (79.2%)	-30.5 (74.3%)	-23.0 (72.3%)	-33.8 (78.9%)	-29.7 (73.4%)	-29.4 (70.1%)	-30.2 (75.3%)	-16.9 (69.4%)	-19.0 (71.5%)	-18.1 (68.2%)
$\Delta E_{orb\ rest}$ [b]	-10.0 (25.4%)	-9.4 (27.7%)	-9.1 (20.8%)	-10.5 (25.7%)	-8.8 (27.7%)	-9.0 (21.1%)	-10.8 (26.6%)	-12.5 (29.9%)	-9.9 (24.7%)	-7.4 (30.2%)	-7.6 (28.5%)	-8.4 (31.8%)
ΔE_{prep}	9.3	11.2	13.4	10.2	9.2	11.8	10.5	14.4	10.1	5.2	6.7	5.9
ΔE ($-D_e$)	21.2	24.6	16.7	20.9	24.0	18.4	23.2	27.9	21.6	27.7	23.0	30.6
d(E-C^{NHC})	260.9	265.5	250.1	258.9	269.1	251.3	260.5	257.8	258.6	282.1	279.4	279.4

[a] The values in parenthesis give the percentage contribution to the total attractive interactions $\Delta E_{elstat} + \Delta E_{orb} + \Delta E_{disp}$. [b] The values in parenthesis give the percentage contribution to the total orbital interactions ΔE_{orb}.

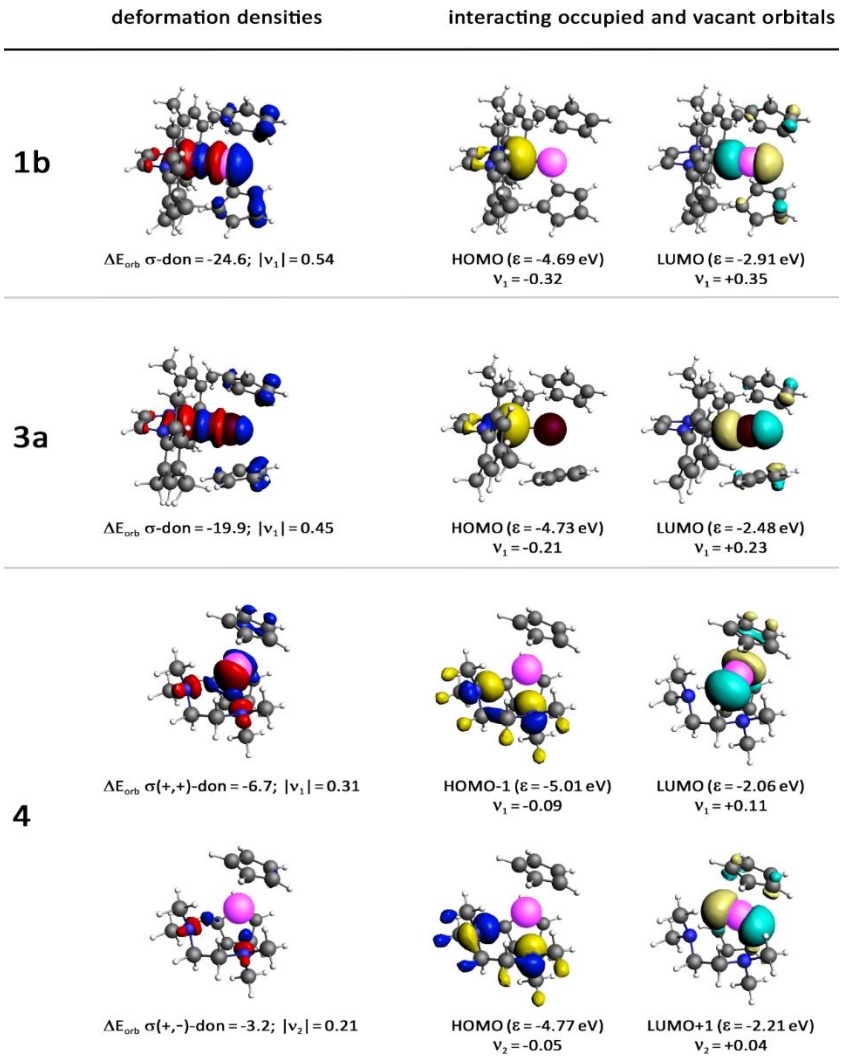

Figure 5. Left: Isodensity plots of deformation densities Δρ (isovalue 0.001 a.u.) of the pairwise orbital interactions between Cp_2E (E = Sn, Pb) moiety and the coordinating ligand (L = NHC^{Mes}, tmeda) for **1b**, **3a** and **4**, and associated energies ΔE (in kcal mol^{-1}) and eigenvalues ν (in a.u.). Red color shows charge outflow and blue color shows charge density accumulation. Center & right: Isodensity plots of the most relevant interacting occupied and vacant orbitals (isovalue 0.05 a.u.) of the fragments.

EDA results also suggest that the bonding interactions are on average 60% ionic and 30% covalent with 10% attractive dispersion interactions for the tin compounds, while in the lead compounds the dispersion interactions have higher relevance, with the bonding interactions on average being 50% ionic, 30% covalent and around 20% dispersion interactions. The ΔE_{disp} term values correlate with the bond energy (D_e) for each series, Sn and Pb (Table 3). For instance, in the tin complexes, values of -22.3 to -25.4 kcal mol^{-1} are calculated as dispersion interaction for complexes with mesityl substituted NHCs, -17.0 kcal mol^{-1} for complexes with NHCs carrying isopropyl groups and only -10.8 to -15.3 kcal mol^{-1} for complexes with methyl-substituted carbenes. This highlights the importance of the dispersion interaction for the stability of the complexes. On the other hand, the covalent contribution, which is ca -40.0 kcal mol^{-1} in case of the tin complexes and -25.0 kcal mol^{-1} in case of the lead complexes, which represents ~33% and ~28% of the stabilizing interaction, respectively. A more detailed insight into the nature of the covalent interactions available from the EDA can be gained in combination with Natural Orbitals for Chemical Valence calculations (EDA-NOCV).[30-33] This method decomposes the orbital term ΔE_{orb} into components $\Delta E_{orb\,\rho(i)}$ that provide the energetic estimation of a given deformation density $\rho_{(i)}$ which is related with a particular electron flow channel, and also the amount of charge transferred $\Delta q_{(i)} = |\nu_{(i)}|$ for the bonding between the interacting fragments (Table 2). For compounds **1-3**, the main deformation densities are associated with the main orbital interactions (Figure 5; Figure S17). The eigenvalues ν, are a measure for the amount of electrons flowing from one orbital to the other (pairwise). According to this data the main contributions in case of **1b** and **3a** are associated with the donation of the lone pairs into the vacant *p* orbitals of the stannocene and plumbocene moiety. The corresponding energies represents around 75% of the total orbital interaction energies. The remaining orbital interactions are attributed to polarization effects. Noteworthy, there is no significant contribution of π-back donation in these NHC complexes, which has been suggested before based on the solid state structures of stannocene NHC complexes,[9] as the carbene ligands relative positions make an interaction between the stannocene lone pair the formally empty *p* orbital of the NHC impossible. We have recently observed such a behavior when low energy gain by π-backdonation is combined with steric hindrance.[10]

We have taken compounds **4** and **5a,b** to compare the coordination mode. NBO results in Table 1 reveal that the metallocene moieties bear less negative charge than in complexes **1-3**. The hybridization indicates that two valence electrons of the metal center are in an *s* orbital and hence the *p* orbital is able to participate in donor-acceptor interactions. The EDA-NOCV values are summarized in Table 3, while the deformation densities assigned to the orbital interactions are shown in Figure 5. The computed dissociation energies (D_e kcal mol^{-1}) for **4** and **5a,b** are around 10 kcal mol^{-1} higher than those reported by Armstrong *et al.*[16] Comparison with the carbene complexes **1-3** suggest even weaker interactions by around 2 kcal mol^{-1}. As in the former complexes, the lead complex **5a** exhibits a stronger bond than its tin analogue **4**. Further inspection is given by the preparation and interaction energies. In this case, the energy penalty to deform the fragment to get into the interacting structure is very low and comparable, namely, 4.1 and 4.0 kcal mol^{-1} for **4** and **5a**, respectively. The small binding energy difference comes from the interaction energy (4.7 kcal mol^{-1}). The EDA dissection results in higher Pauli repulsion for the lead complex but also higher stabilization interactions. Herein, dispersion interaction contributes with 30% to the total stabilization interaction, while the electrostatic and orbital contribute around 45% and 25%, respectively. Interestingly, these complexes present two main orbital contributions which come from the positive combination of the nitrogen atoms lone pairs (+,+) combination which interact with the one of the empty *p* orbital of the metallocene, and a (+,–) lone pair combination that donates electrons into the other vacant *p*-orbital (Figure 5). These orbital interactions are possible due to the low hybridization degree of the stannocene and plumbocene metal centers. Note that the orbital interaction is slightly higher in line with the shorter Pb-N distances (Figure 3).

Table 3. Energy decomposition analysis (EDA-NOCV) of the E-N^{ligand} bond (E = Sn, Pb) in compounds 4,5 at BP86+D3(BJ)/ZORA&TZ2P level of theory. Energy values are given in kcal mol^{-1}.

	4	5a	5b
ΔE_{int}	-20.1	-24.8	-21.0
ΔE_{Pauli}	31.2	35.9	29.9
ΔE_{elstat}[a]	-21.4 (41.7%)	-27.6 (45.5%)	-24.2 (47.5%)
ΔE_{disp}[a]	-16.2 (31.5%)	-17.4 (28.6%)	-13.5 (26.6%)
ΔE_{orb}[a]	-13.8 (26.9%)	-15.7 (25.9%)	-13.2 (25.9%)
$\Delta E_{orb\,(+,+)\,\sigma\text{-don}}$[b]	-6.7 (48.9%)	-7.7 (48.8%)	-7.3 (55.2%)
$\Delta E_{orb\,(+,-)\,\sigma\text{-don}}$[b]	-3.2 (23.0%)	-3.7 (23.7%)	-2.3 (17.3%)
$\Delta E_{orb\,rest}$[b]	-3.9 (28.2%)	-4.3 (27.6%)	-3.6 (27.5%)
ΔE_{prep}	4.1	4.0	1.7
ΔE ($-D_e$)	16.0	20.8	19.3

[a] The values in parenthesis give the percentage contribution to the total attractive interactions $\Delta E_{elstat} + \Delta E_{orb} + \Delta E_{disp}$. [b] The values in parenthesis give the percentage contribution to the total orbital interactions ΔE_{orb}.

As aforementioned, the tetrelocene-NHC complexes are significantly more reactive than their initial reactants. This is related with a general observation of longer Cp-E bond lengths upon complexation of the NHC to the metal center or any other ligand. To understand the origins of this observation, we have used a model where the side substituents on the nitrogen atoms are replaced by hydrogen atoms. This is the smallest substituent possible for the NHC ligands. Note that in this case, the carbene disposes in a different manner since the steric hindrance is reduced significantly. Our calculations suggest Cp-E dissociation energies of 549.3 and 526.0 kcal mol^{-1} for stannocene (Cp_2Sn) and plumbocene (Cp_2Pb), respectively. Upon complexation with NHC, the dissociation energy is reduced by more than 100 kcal mol^{-1}, i.e. 411.0 and 404.8 kcal mol^{-1} for Sn and Pb complexes, respectively. In terms of bond distances, the Sn-Cp bond length is elongated from 246.9 to 279.7 pm upon complexation, while Cp-Pb is lengthened from 254.7 to 266.4 pm. Notably, this affects more strongly the stannocene complexes than the

plumbocene complexes. These observations have been ascribed to the donation of the lone pair into the *p* orbital of the metal center which has antibonding interaction with the Cp groups.[34] We have used EDA on the metal center and Cp group interaction to unravel the origins of such a change. Thus, we have considered a fragmentation scheme where one of the fragments is the E^{2+} or $(E\text{-NHC})^{2+}$ and the other is $(Cp^-)_2$ (Scheme 2, Table S4). Our results are in good agreement with previous calculations by Rayón *et al.* on metallocenes chemical bonding.[35] The bonding for metallocenes is 70% ionic and 28% covalent with a small dispersion interaction contribution of 2%. The main orbital terms are related to the electron donation of the Cp^- groups to the E^{2+} element. Our results suggest that the lowering of the dissociation energy comes primarily from a weaker interaction energy ΔE_{int}. The stabilization interaction decreases upon complexation since the electrostatic and orbital interactions are weaker. On the one hand, the electrostatic interaction energy decreases by around 70 kcal mol^{-1} since the metal center receives electrons from the carbene ligand. On the other hand, the orbital interaction decreases by ca. 50 kcal mol^{-1} due to weaker donations to the *p* orbitals of the metal center.

Scheme 2. Cp-E (E = Sn, Pb) dissociation energies (D_e) of metallocenes and metallocene-NHC complexes at B3LYP+D3/def2-TZVP.

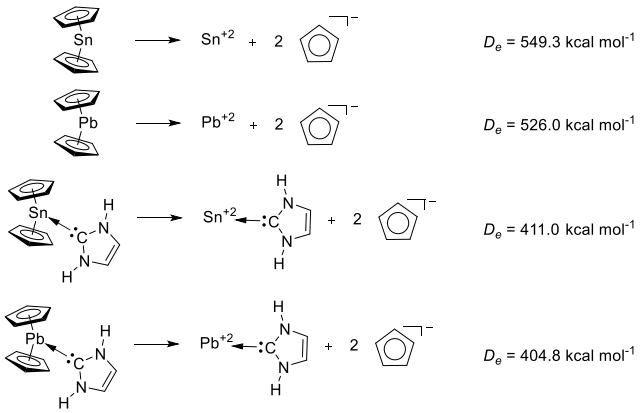

Aside from the metallocene-NHC complexes, dispersion interactions have previously also been described to be very important in case of Si[2]stannocenophane, as the compound exists as a dimer in the solid state, which is believed to be caused by attractive dispersion interactions, rather than a "classical" Sn-Sn bond, as indicated by solution and solid state CP-MAS ^{119}Sn NMR spectroscopy.[36] The ^{119}Sn Mössbauer spectrum of the sila[2]stannocenophane recorded at 6 K (Figure 6) supports this assumption. The spectrum is well reproduced with a single signal at an isomer shift of δ = 3.734(6) mm s^{-1}, subjected to electric quadrupole splitting of ΔE_Q = 1.00(1) mm s^{-1}. The experimental line width parameter of Γ = 1.08(2) mm s^{-1} is slightly enhanced.

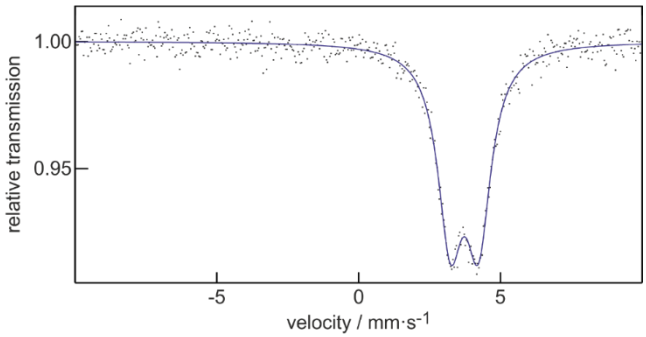

Figure 6. Experimental and simulated ^{119}Sn Mössbauer spectrum of sila[2]stannocenophane at 6 K.

Although, as aforementioned, the crystal structure contains two crystallographically independent tin sites, they cannot be distinguished in the ^{119}Sn Mössbauer spectrum. Both tin sites exhibit an almost similar electronic environment and the envelope is observed. This is expressed by the slightly enhanced line width parameter. Significantly, the isomer shift of sila[2]stannocenophane is close to that reported for stannocene (δ = 3.73(6) mm s^{-1}),[37, 38] which means sila[2]stannocenophane does not exhibit any covalent Sn-Sn bond and can be regarded as a divalent tin compound.[39] The electric quadrupole splitting parameter for sila[2]stannocenophane is increased, compared to that of stannocene (ΔE_Q = 0.65(6) to 1.00(1) mm s^{-1}).[37] This is a consequence of the tilt of the Cp ligands due to the *ansa*-bridging, leading to a more asymmetric electron density at the tin nuclei in sila[2]stannocenophane.

We have performed EDA-NOCV calculations to understand the physical factors controlling the interaction between the two sila[2]stannocenophane units (Table S5). EDA suggest that dissociation energy for the dimer is indeed very weak, namely -7.6 kcal mol^{-1}. The dissection of the interaction energy discloses that the main contribution is dispersion interaction (63.1%) while the electrostatic and covalent contribution are very small, 19.4% and 17.5%, respectively. To examine the origins of the dispersion interaction, we have performed energy partitioning within the local correlation methods.[40] We have generated potential energy plot by the displacement of the sila[2]stannocenophane monomers away from each other from 300 to 700 pm (Chart 2, Figure 7).

Chart 2. Si[2]stannocenophane dispersion-dimer

Note that HF/cc-pVTZ predicts no interaction between the monomers. This is in agreement with the EDA calculations which show weak electrostatic interaction. The effect of correlation is given by the difference of the calculated curves to the HF curve. The SCS-LMP2/cc-pVTZ[41] curves predict an equilibrium distance of 460 pm, while the LMP2/cc-pVTZ gives shorter distance, i.e., 440 ppm. This is expected, since MP2 tends to overestimate dispersion interactions.[42-47] The curves nevertheless are very similar, with an energy of -3.6 kcal mol^{-1} and -2.3 kcal mol^{-1}, but a shorter equilibrium distance.

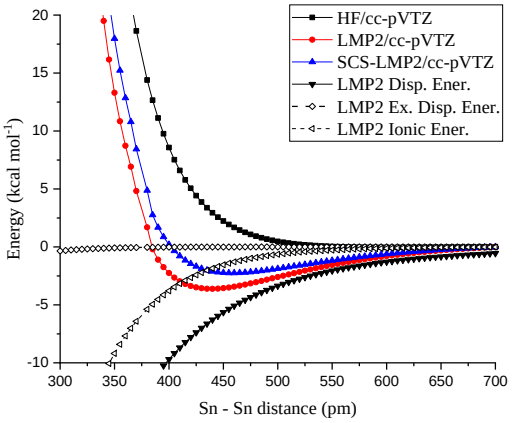

Figure 7. Potential energy curve of the interaction between the sila[2]stannocenophane units. The energy values are given as a function of the Sn1–Sn2 distance.

The local character of occupied and virtual orbitals in the local correlation treatments offers the possibility to dissect intramolecular effects (double excitations from occupied orbitals of one unit into virtual orbitals of the same unit) from intermolecular ones (excitations involving orbitals from both units).[40] Additionally, the intermolecular correlation effects can be decomposed according to different excitation classes: dispersion effects originate from simultaneous mono-excitations at each unit, exchange-dispersion is similar but the mono-excitations are from the occupied space of one unit to the virtual space of the other and vice versa; ionic contributions come from mono-excitations from the occupied space of both units into the virtual space of only one of them. The different classes have been discussed in detail by Schütz *et al.*[40, 48, 49] In Figure 7, together with the energy curves, each intermolecular contribution term is also displayed as a function of the distance between the tin atoms. These curves show a continuous favorable interaction with decreasing distance. The main contribution interaction to the correlation energy is the dispersion (-6.6 kcal mol^{-1}) while the ionic excitation and exchange dispersion effects are -0.01 and -2.0 kcal mol^{-1}, respectively.

CONCLUSION

In this work, a series of stannocene and plumbocene N-heterocyclic carbene complexes have been studied experimentally and computationally. Their key chemical bonds have been described by Energy Decomposition Analysis. The results suggest that the binding is coordinative having a strong dispersion interaction contribution. The orbital interaction occurs mainly from the donation of the carbene lone pair into the empty p orbital of tin or lead. Remarkably, the carbene ligand disposition towards the main metal center is dominated by the volume of the group on the nitrogen atoms, which preclude the π-back-donation. The complexation weakens the interaction of the metal with the cyclopentadienyl moieties by ca. 100 kcal mol^{-1} and lengthen the E-Cp bonds significantly, by up to ~25 pm. This has been ascribed to the occupation of the LUMO which has an antibonding interaction nature with the cyclopentadienyl groups. Dispersion interactions are also the ruling effect to form stannocene dimers for the Si[2]stannocenophane derivatives, where no chemical bond has been found between the tin atoms.

EXPERIMENTAL SECTION

All manipulations were carried out under an inert gas atmosphere (argon 5.0), using either Schlenk line techniques or a glovebox. 1,3,4,5-tetramethyl-imidazol-2-ylidene,[50] 1,3-dimesityl-imidazol-2-ylidene,[51] Si[2]stannocenophane[36] and plumbocene[52] were prepared following literature known procedures. Deuterated benzene was purchased from ABCR and dried over 400 pm molecular sieves. NMR-spectra were recorded on Bruker Avance III 300 (solution NMR), Bruker Avance III 400 (solution NMR) and Bruker Ascend 400WB (solid state NMR) spectrometers. ^{1}H and ^{13}C NMR spectra were referenced using the solvent signals.[53] ^{29}Si, ^{119}Sn and ^{207}Pb NMR spectra were referenced using external standards (δ^{29}Si(SiMe$_4$) = 0; δ^{119}Sn(SnMe$_4$) = 0; δ^{207}Pb(PbMe$_4$) = 0). Elemental analysis were performed with an Elementar vario microcube. Single crystal X-ray diffraction analyses were carried out at low temperatures on a Bruker AXS X8 Apex CCD and Bruker AXS D8 Venture diffractometer operating with graphite monochromated Mo Kα radiation. Structure solution and refinement were performed using SHELX.[54] The ^{119}Sn Mössbauer spectroscopy was performed with a Ca^{119m}SnO$_3$ source. Ca. 240 mg of the sample was placed within a thin-walled PMMA container. A palladium foil of 0.05 mm thickness was used to reduce the tin K X-rays concurrently emitted by this source. The measurement (10 d total counting time) was conducted in a continuous flow cryostat system (Janis Research Co LLC) at 6 K. The spectrum was fitted with the NORMOS-90 software package.[55]

Synthesis of 2a.

2 mL of toluene, precooled to 193 K, were added to a mixture of Si[2]stannocenophane (200 mg, 551 µmol) and 1,3,4,5-tetramethylimidazole-2-ylidene (68 mg, 548 µmol). The resulting mixture was stirred for 10 min at 193 K. Storage of this solution at 248 K yielded yellow crystals of stannocenophane carbene complex **2a**.

Yields: 22 mg / 8%.

Elemental Analysis for $C_{21}H_{32}N_2Si_2Sn$: calculated: 51.75% C, 6.62% H, 5.75% N; found: 51.41% C, 6.91% H, 6.04% N.

^{1}H-NMR (400.13 MHz, 296 K, C_6D_6) δ = 0.54 (s, 12 H, Si-C$\underline{H}_3$), 1.28 (s, 6 H, C-C$\underline{H}_3$), 3.05 (s, 6 H, N-C$\underline{H}_3$), 6.14 (t, $^{3}J_{HH}$ = 2 Hz, 4H, Cp-$\underline{H}$), 6.42 (t, $^{3}J_{HH}$ = 2 Hz, 4H, Cp-$\underline{H}$); ^{13}C{^{1}H}-NMR (100.62 MHz, 296 K, C_6D_6) δ = -2.6 (Si-$\underline{C}$H$_3$), 8.0 (C-$\underline{C}$H$_3$), 33.5 (N-$\underline{C}$H$_3$), 114.6 (Cp), 114.7 (Cp), 115.9 ($\underline{C}$=$\underline{C}$), 117.7 (Cp); ^{29}Si{^{1}H}-INEPT-NMR (79.49 MHz, 296 K, C_6D_6) δ = -27.0; No signal could be detected in the ^{119}Sn NMR spectrum in the range of -1650 to -2650 ppm, presumably due to extreme signal broadening.

Synthesis of 3a.

15 mL of toluene were added to a mixture of plumbocene (100 mg, 300 µmol) and 1,3-dimesitylimidazole-2-ylidene (90 mg, 300 µmol). The solution was stirred at room temperature for 10 min and then stored at 248 K overnight, yielding yellow crystals of plumbocene carbene complex **3a**.

Yields: 110 mg / 57%.

Elemental Analysis for $C_{31}H_{34}N_2Pb$: calculated: 58.01% C, 5.34% H, 4.36% N; found: 56.79% C, 5.39% H, 4.13% N (carbon value was repeatedly reproducibly low, even upon analysis of highly crystalline material).

^{1}H-NMR (400.13 MHz, 296 K, C_6D_6) δ = 2.09 (s, 12H, *o*-Mes-C$\underline{H}_3$), 2.13 (s, 6H, *p*-Mes-C$\underline{H}_3$), 5.86 (s, 10H, Cp-$\underline{H}$), 6.24 (s, 2H, NC-$\underline{H}$), 6.79 (s, 4H, *m*-Mes-$\underline{H}$); ^{13}C{^{1}H}-NMR (100.61 MHz, 296 K, C_6D_6) δ = 18.1 (*o*-Mes-$\underline{C}$H$_3$), 21.0 (*p*-Mes-$\underline{C}$H$_3$), 110.8 (Cp), 121.0 ($\underline{C}$=$\underline{C}$), 129.4 (Mes), 135.1 (Mes), 137.6 (Mes), 138.3 (Mes), 226.9 (carbene-$\underline{C}$); ^{13}C{^{1}H}-CP/MAS(15 kHz)-NMR (100.65 MHz, 296 K) δ = 17.6 (Mes-$\underline{C}$H$_3$), 21.2 (Mes-$\underline{C}$H$_3$), 24.3 (Mes-$\underline{C}$H$_3$), 109.5, 120.9, 122.1, 128.8, 131.2, 132.4, 133.1, 134.6, 139.2, 239.0 (carbene-$\underline{C}$); ^{207}Pb{^{1}H}-CP/MAS(13 kHz)-NMR (83.37 MHz, 296 K) δ = -4118.

Synthesis of 3c.

A solution of plumbocenophane (100 mg, 214 µmol) in 2 mL of toluene was added to a solution of 1,3-dimesitylimidazole-2-ylidene (66.0 mg, 217 µmol) in 2 mL of toluene and storage of the solution at 248 K yielded yellow crystals of plumbocenophane carbene complex **3c**. Crystals suitable for XRD are obtained from a thf solution at 248 K.

Yields: 127 mg / 77%.
Elemental Analysis for $C_{35}H_{44}N_2OPbSi_2$: calculated: 54.45% C, 5.74 % H, 3.63 % N; found: 54.83% C, 5.70% H, 3.42% N.
^{1}H-NMR (400.13 MHz, 293 K, C_6D_6) δ = 0.45 (s, 12H, Si-C$\underline{H}_3$), 2.04 (s, 12H, *o*-Mes-C$\underline{H}_3$), 2.17 (s, 6H, *p*-Mes-C$\underline{H}_3$), 6.02-6.05 (m, 8H, Cp-$\underline{H}$), 6.13 (s, 2H, N-C$\underline{H}$), 6.81 (s, 4H, *m*-Mes-$\underline{H}$); ^{13}C{^{1}H}-NMR (100.63 MHz, 293 K, C_6D_6) δ = 2.2 (Si-$\underline{C}$H$_3$), 18.0 (*o*-Mes-$\underline{C}$H$_3$), 21.1 (*p*-Mes-$\underline{C}$H$_3$), 113.9 (Cp), 116.6 (Cp), 121.3 ($\underline{C}$=$\underline{C}$), 129.6 (Mes), 135.0 (Mes), 136.6 (Mes), 138.9 (Mes), 229.7 (carbene-C); ^{13}C{^{1}H}-CP/MAS(13 kHz)-NMR (100.67 MHz, 297 K) δ = 0.3 (Si-$\underline{C}$H$_3$), 2.8 (Si-$\underline{C}$H$_3$), 17.7 (Mes-$\underline{C}$H$_3$), 19.2 (Mes-$\underline{C}$H$_3$), 23.3 (Mes-$\underline{C}$H$_3$), 108.4, 110.7, 112.5, 117.6, 121.6, 123.5, 124.3, 130.5, 133.0, 135.7, 140.2, 238.8 (carbene-$\underline{C}$); ^{29}Si{^{1}H}-INEPT-NMR (59.63 MHz, 296 K, C_6D_6) δ = -7.0; ^{207}Pb{^{1}H}-NMR (62.51 MHz, 295 K, C_6D_6) δ = -4344.

Computational Details

All geometries were optimized without symmetry constraint within the DFT (density functional theory) framework using the B3LYP[56, 57] and BP86 functionals[58, 59] in combination with the Grimme Dispersion corrections using the Becke-Johnson damping function D3(BJ)[60, 61] and the Ahlrichs def2-TZVP basis function.[62] These calculations were performed using the Gaussian 16 A03 software suite.[63] The stationary points were located with the Berny algorithm[64] using redundant internal coordinates. Analytical Hessians were computed to determine the nature of stationary points (one and zero imaginary frequencies for transition states and minima, respectively)[65] and to calculate unscaled zero-point energies (ZPEs) as well as thermal corrections and entropy effects using the standard statistical-mechanics relationships for an ideal gas.[66] Unless otherwise stated, Gibbs energies have been computed at 298.15 K. The Wiberg Bond Indices (WBI)[67] and NPA[68, 69] atomic partial charges have been calculated at the BP86+D3/def2-TZVP level using GENNBO6.0 programs.[70] The nature of the chemical bonds were investigated by means of the Energy Decomposition Analysis (EDA) method, which was developed by Morokuma[24] and by Ziegler and Rauk.[25, 71] The bonding analysis focuses on the instantaneous interaction energy ΔE_{int} of a bond A-B between two fragments A and B in the particular electronic reference state and in the frozen geometry AB. This energy is divided into four main components (Eq 2).

$$\Delta E_{\text{int}} = \Delta E_{elst} + \Delta E_{Pauli} + \Delta E_{orb} + \Delta E_{disp} \quad (1)$$

The term ΔE_{elst} corresponds to the classical electrostatic interaction between the unperturbed charge distributions of the prepared atoms (or fragments) and it is usually attractive. The Pauli repulsion ΔE_{Pauli} is the energy change associated with the transformation from the superposition of the unperturbed wave functions (Slater determinant of the Kohn-Sham orbitals) of the isolated fragments to the wave function $\Psi_0 = N\hat{A}[\Psi_A\Psi_B]$, which properly obeys the Pauli principle through explicit antisymmetrization ($\hat{A}$ operator) and renormalization (N = constant) of the product wave function. It comprises the destabilizing interactions between electrons of the same spin on either fragment. The orbital interaction ΔE_{orb} accounts for charge transfer and polarization effects.[72] In the case that the Grimme dispersion corrections[60, 61] are computed the term ΔE_{disp} is added to the equation 2. Further details on the EDA method can be found in the literature.[26, 73] In the case of the dimers the relaxation of the fragments to their equilibrium geometries at the electronic ground state is termed ΔE_{prep}, because it may be considered as preparation energy for chemical bonding. The addition of ΔE_{prep} to the intrinsic interaction energy ΔE_{int} gives the total energy ΔE, which is - by definition with opposite sign - the bond dissociation energy D_e:

$$\Delta E(-D_e) = \Delta E_{\text{int}} + \Delta E_{prep} \quad (2)$$

The EDA–NOCV method combines the EDA with the natural orbitals for chemical valence (NOCV) to decompose the orbital interaction term ΔE_{orb} into pairwise contributions. The NOCVs Ψ_i are defined as the eigenvector of the valence operator, $\hat{V}$, given by Equation (3).

$$\hat{V}\Psi_i = \nu_i\Psi_i \quad (3)$$

In the EDA–NOCV scheme the orbital interaction term, ΔE_{orb}, is given by Equation (4),

$$\Delta E_{\text{orb}} = \sum_k \Delta E = \sum_{k=1}^{N/2}\left[-F_{-k,k}^{TS} + F_{k,k}^{TS}\right] \quad (4)$$

in which $F_{-k,-k}^{TS}$ and $F_{k,k}^{TS}$ are diagonal transition state Kohn–Sham matrix elements corresponding to NOCVs with the eigenvalues $-\nu_k$ and ν_k, respectively. The ΔE_k^{orb} term for a particular type of bond is assigned by visual inspection of the shape of the deformation density $\Delta\rho_k$. The latter term is a measure of the size of the charge deformation and it provides a visual notion of the charge flow that is associated with the pairwise orbital interaction. The EDA–NOCV scheme thus provides both qualitative and quantitative information about the strength of orbital interactions in chemical bonds. The EDA-NOCV calculations were carried out with ADF2018.[73] the basis sets for all elements have triple-ζ quality augmented by two sets of polarizations functions and one set of diffuse function. Core electrons were treated by the frozen-core approximation. This level of theory is denoted BP86+D3(BJ)/TZ2P.[74] Scalar relativistic effects have been incorporated by applying the zeroth-order regular approximation (ZORA).[75] We performed the second-order local Møller-Plesset perturbation theory (LMP2)[76-84] levels of theory calculations by employing MOLPRO 2019.1[85] software program package. Density fitting (DF) approximations have been used in this local method.[86] The cc-pVTZ basis set was used for carbon, silicon and tin while for hydrogen the cc-pVTZ basis set was used.[87, 88] In the density fitting calculations reported in this paper, we used the cc-pVTZ/JKJIT and cc-pVTZ/MP2FIT auxiliary fitting basis sets43 in the DF-HF and DF-LMP2 calculations, respectively. The LMP2 calculations were carried out using Pipek-Mezey localized orbitals.[86] The domains were determined with the use of natural population analysis criteria, with TNPA = 0.03.

ASSOCIATED CONTENT

Supporting Information

The Supporting Information is available free of charge on the ACS Publications website.
crystallographic details, NMR spectra, computational details (PDF)
optimized geometries (xyz)

AUTHOR INFORMATION

Corresponding Author

*E-mail: diego.andrada@uni-saarland.de (D.M.A.)
*E-mail: andre.schaefer@uni-saarland.de (A.S.)
*E-mail: pottgen@uni-muenster.de (R.P.)

ORCID

Diego M. Andrada: 0000-0003-2515-7859
André Schäfer: 0000-0002-5969-6618
Rainer Pöttgen: 0000-0003-0962-279X
Sergi Danés: 0000-0003-4777-0398
Carsten Müller: 0000-0002-4702-2202

Author Contributions

§ S.D., C.M. and L.W. have contributed equally. Names are given in alphabetical order.

Notes

The authors declare no competing financial interest.

ACKNOWLEDGMENT

D.M.A. and A.S. thank Prof. Dr. David Scheschkewitz, Prof. Dr. Guido Kickelbick and Saarland University for support. D.M.A thanks the European Research Council, ERC, (ERC Starting grants, EU805113) for funding. A.S. thanks the Deutsche Forschungsgemeinschaft, DFG, (Emmy Noether-program, SCHA1915/3-1) and the Fonds der Chemischen Industrie, FCI, for funding.

REFERENCES

1. Arduengo III, A. J.; Harlow, R. L.; Kline, M., A stable crystalline carbene. *J. Am. Chem. Soc.* **1991,** *113*, 361-363.
2. Wanzlick, H. W.; Schönherr, H. J., Direct Synthesis of a Mercury Salt-Carbene Complex *Angew. Chem. Int. Ed.* **1968,** *7*, 141-142.
3. Nesterov, V.; Reiter, D.; Bag, P.; Frisch, P.; Holzner, R.; Porzelt, A.; Inoue, S., NHCs in Main Group Chemistry. *Chem. Rev.* **2018,** *118*, 9678-9842.
4. Doddi, A.; Peters, M.; Tamm, M., N-Heterocyclic Carbene Adducts of Main Group Elements and Their Use as Ligands in Transition Metal Chemistry. *Chem. Rev.* **2019,** *119*, 6994-7112.
5. Kundu, S.; Sinhababu, S.; Chandrasekhar, V.; Roesky, H. W., Stable cyclic (alkyl)(amino)carbene (cAAC) radicals with main group substituents. *Chem. Sci.* **2019,** *10*, 4727-4741.
6. Frenking, G.; Hermann, M.; Andrada, D. M.; Holzmann, N., Donor-acceptor bonding in novel low-coordinated compounds of boron and group-14 atoms C-Sn. *Chem. Soc. Rev.* **2016,** *45*, 1129-1144.
7. Soleilhavoup, M.; Bertrand, G., Cyclic (Alkyl)(Amino)Carbenes (CAACs): Stable Carbenes on the Rise. *Acc. Chem. Res.* **2015,** *48*, 256-266.
8. Melaimi, M.; Jazzar, R.; Soleilhavoup, M.; Bertrand, G., Cyclic (Alkyl)(amino)carbenes (CAACs): Recent Developments. *Angew. Chem. Int. Ed.* **2017,** *56*, 10046-10068.
9. Müller, C.; Stahlich, A.; Wirtz, L.; Gretsch, C.; Huch, V.; Schäfer, A., Carbene Complexes of Stannocenes. *Inorg. Chem.* **2018,** *57*, 8050-8053.
10. Müller, C.; Andrada, D. M.; Bischoff, I.-A.; Zimmer, M.; Huch, V.; Steinbrück, N.; Schäfer, A., Synthesis, Structure, and Bonding Analysis of Tin(II) Dihalide and Cyclopentadienyltin(II) Halide (Alkyl)(amino)carbene Complexes. *Organometallics* **2019,** *38*, 1052-1061.
11. Rottschäfer, D.; Sharma, M. K.; Neumann, B.; Stammler, H.-G.; Andrada, D. M.; Ghadwal, R. S., A Modular Access to Divinyldiphosphenes with a Strikingly Small HOMO–LUMO Energy Gap. *Chem. Eur. J.* **2019,** *25*, 8127-8134.
12. Wirtz, L.; Jourdain, M.; Huch, V.; Zimmer, M.; Schäfer, A., Synthesis, Structure and Reactivity of Disiloxa[3]tetrelocenophanes. *ACS Omega* **2019**.
13. Müller, C.; Andrada, D. M.; Bischoff, I.-A.; Zimmer, M.; Huch, V.; Steinbrück, N.; Schäfer, A., Synthesis, Structure, and Bonding Analysis of Tin(II) Dihalide and Cyclopentadienyltin(II) Halide (Alkyl)(amino)carbene Complexes. *Organometallics* **2019**.
14. Feixas, F.; Matito, E.; Poater, J.; Sola, M., Quantifying aromaticity with electron delocalisation measures. *Chem. Soc. Rev.* **2015,** *44*, 6434-6451.
15. Beswick, M. A.; Cromhout, N. L.; Harmer, C. N.; Raithby, P. R.; Russel, C. A.; Smith, J. S. B.; Steiner, A.; Wright, D. S., Loosely bonded adducts of plumbocene; Structure and solution dynamics of $[(\eta\text{-}C_5H_5)_2Pb.(tmeda)]$ and $[(\eta\text{-}C_5H_5)_2Pb.4,4'\text{-}Me_2bipy]$ (tmeda=$Me_2NCH_2CH_2NMe_2$,4,4'-Me_2bipy=4,4'-dimethylbipyridine). *Chem. Comm.* **1996**, 1977-1978.
16. Armstrong, D. R.; Beswick, M. A.; Cromhout, N. L.; Harmer, C. N.; Moncrieff, D.; Russell, C. A.; Raithby, P. R.; Steiner, A.; Wheatley, A. E. H.; Wright, D. S., Weakly bonded Lewis base adducts of plumbocene and stannocene: A synthetic and calculational study. *Organometallics* **1998,** *17*, 3176-3181.
17. Hey, J.; Andrada, D. M.; Michel, R.; Mata, R. A.; Stalke, D., Strong intermolecular interactions shaping a small piano-stool complex. *Angew. Chem. Int. Ed.* **2013,** *52*, 10365-10369.
18. Singh, A. P.; Samuel, P. P.; Mondal, K. C.; Roesky, H. W.; Sidhu, N. S.; Dittrich, B., Lewis Base Stabilized Group 14 Metalylenes. *Organometallics* **2013,** *32*, 354-357.
19. Bantu, B.; Pawar, G. M.; Decker, U.; Wurst, K.; Schmidt, A. M.; Buchmeiser, M. R., CO_2 and SnII Adducts of N-Heterocyclic Carbenes as Delayed-Action Catalysts for Polyurethane Synthesis. *Chem. Eur. J.* **2009,** *15*, 3103-3109.
20. Bessac, F.; Frenking, G., Chemical bonding in phosphane and amine complexes of main group elements and transition metals. *Inorg. Chem.* **2006,** *45*, 6956-6964.
21. Loschen, C.; Voigt, K.; Frunzke, J.; Diefenbach, A.; Diedenhofen, M.; Frenking, G., Theoretical studies of inorganic compounds. 19 Quantum chemical investigations of the phosphane complexes $X_3B\text{-}PY_3$ and $X_3Al\text{-}PY_3$ (X = H, F, Cl; Y = F, Cl, Me, CN). *Z. Anorg. Allg. Chem.* **2002,** *628*, 1294-1304.
22. Wagner, J. P.; Schreiner, P. R., London Dispersion in Molecular Chemistry-Reconsidering Steric Effects. *Angew. Chem. Int. Ed.* **2015,** *54*, 12274-12296.
23. Liptrot, D. J.; Power, P. P., London dispersion forces in sterically crowded inorganic and organometallic molecules. *Nat. Rev. Chem.* **2017,** *1*, 1.
24. Morokuma, K., Moluecular orbital studies of hydrogen bonds 3. C=O H-O hydrogen bond in H_2CO and H_2O and H_2CO $2H_2O$. *J. Chem. Phys.* **1971,** *55*, 1236-1244.
25. Ziegler, T.; Rauk, A., CO, CS, N_2, PF_3, and $CNCH_3$ as σ-donors and π-acceptors - Theoretical-study by the Hartree-Fock-Slater Transition-State method. *Inorg. Chem.* **1979,** *18*, 1755-1759.
26. Bickelhaupt, F. M.; Baerends, E. J., Kohn-Sham density functional theory: Predicting and understanding chemistry. In *Reviews in Computational Chemistry*, Lipkowitz, K. B.; Boyd, D. B., Eds.2000; Vol. 15, pp 1-86.
27. Tonner, R.; Frenking, G., Divalent carbon(0) chemistry, part 1: Parent compounds. *Chem. Eur. J.* **2008,** *14*, 3260-3272.
28. Andrada, D. M.; Frenking, G., Stabilization of Heterodiatomic SiC Through Ligand Donation: Theoretical Investigation of $SiC(L)_2$ (L = NHCMe, CAAC(Me), PMe_3). *Angew. Chem. Int. Ed.* **2015,** *54*, 12319-12324.
29. Engelhardt, F.; Maaß, C.; Andrada, D. M.; Herbst-Irmer, R.; Stalke, D., Benchmarking lithium amide versus amine bonding by charge density and energy decomposition analysis arguments. *Chem. Sci.* **2018**.
30. Michalak, A.; Mitoraj, M.; Ziegler, T., Bond orbitals from chemical valence theory. *J. Chem. Phys. A* **2008,** *112*, 1933-1939.
31. Mitoraj, M.; Michalak, A., Donor-acceptor properties of ligands from the natural orbitals for chemical valence. *Organometallics* **2007,** *26*, 6576-6580.
32. Mitoraj, M.; Michalak, A., Applications of natural orbitals for chemical valence in a description of bonding in conjugated molecules. *J. Mol. Model.* **2008,** *14*, 681-687.
33. Mitoraj, M. P.; Michalak, A.; Ziegler, T., A Combined Charge and Energy Decomposition Scheme for Bond Analysis. *J. Chem. Theory Comput.* **2009,** *5*, 962-975.
34. Jutzi, P.; Burford, N., Structurally diverse pi-cyclopentadienyl complexes of the main group elements. *Chem. Rev.* **1999,** *99*, 969-990.
35. Rayón, V. M.; Frenking, G., Structures, bond energies, heats of formation, and quantitative bonding analysis of main-group metallocenes [E(Cp)2] (E=Be-Ba, Zn, Si-Pb) and [E(Cp)] (E=Li-Cs, B-Tl). *Chem. Eur. J.* **2002,** *8*, 4693-4707.
36. Schafer, A.; Rohe, K.; Grandjean, A.; Huch, V., Synthesis and Structure of 2 Tetrelocenophanes. *Eur. J. Inorg. Chem.* **2017**, 35-38.
37. Harrison, P. G.; Zuckerman, J. J., Tin-119m Mössbauer and nuclear magnetic resonance study of Dicyclopentadienyltin(II). *J. Am. Chem. Soc.* **1969,** *91*, 6885-6886.
38. Harrison, P. G.; Healy, M. A., Derivatives of divalent germanium, tin and lead : II. Spectroscopic investigation of dicyclopentadienyltin(II) and its methylcyclopentadienyl analogue. *J. Organomet. Chem.* **1973,** *51*, 153-166.
39. Lippens, P. E., Interpretation of the Sn-119 Mossbauer isomer shifts in complex tin chalcogenides. *Phys. Rev. B* **1999,** *60*, 4576-4586.
40. Schütz, M.; Rauhut, G.; Werner, H. J., Local treatment of electron correlation in molecular clusters: Structures and stabilities of (H2O)n, n = 2-4. *J. Phys. Chem. A* **1998,** *102*, 5997-6003.
41. Saebø, S.; Pulay, P., Local configuration interaction: An efficient approach for larger molecules. *Chem. Phys. Lett.* **1985,** *113*, 13-18.
42. Hill, J. G.; Platts, J. A.; Werner, H. J., Calculation of intermolecular interactions in the benzene dimer using coupled-cluster and

local electron correlation methods. *Phys. Chem. Chem. Phys.* **2006,** *8*, 4072-4078.

43. Grimme, S., On the importance of electron correlation effects for the π-π interactions in cyclophanes. *Chem. Eur. J.* **2004,** *10*, 3423-3429.

44. Piacenza, M.; Grimme, S., Van der Waals complexes of polar aromatic molecules: Unexpected structures for dimers of azulene. *J. Am. Chem. Soc.* **2005,** *127*, 14841-14848.

45. Piacenza, M.; Grimme, S., Van der Waals interactions in aromatic systems: Structure and energetics of dimers and trimers of pyridine. *ChemPhysChem* **2005,** *6*, 1554-1558.

46. Takatani, T.; David Sherrill, C., Performance of spin-component-scaled Møller-Plesset theory (SCS-MP2) for potential energy curves of noncovalent interactions. *Phys. Chem. Chem. Phys.* **2007,** *9*, 6106-6114.

47. Van Mourik, T.; Wilson, A. K.; Dunning Jr, T. H., Benchmark calculations with correlated molecular wavefunctions. XIII. Potential energy curves for He_2, Ne_2 and Ar_2 using correlation consistent basis sets through augmented sextuple zeta. *Mol. Phys.* **1999,** *96*, 529-547.

48. Bistoni, G., Finding chemical concepts in the Hilbert space: Coupled cluster analyses of noncovalent interactions. *WIREs* **2019,** *0*, e1442.

49. Schneider, W. B.; Bistoni, G.; Sparta, M.; Saitow, M.; Riplinger, C.; Auer, A. A.; Neese, F., Decomposition of Intermolecular Interaction Energies within the Local Pair Natural Orbital Coupled Cluster Framework. *J. Chem. Theory Comput.* **2016,** *12*, 4778-4792.

50. Kuhn, N.; Kratz, T., Synthesis of imidazol-2-ylidenes by reduction of imidazole-2(3H)-thiones. *Synthesis-Stuttgart* **1993**, 561-562.

51. Arduengo, A. J.; Krafczyk, R.; Schmutzler, R.; Craig, H. A.; Goerlich, J. R.; Marshall, W. J.; Unverzagt, M., Imidazolylidenes, imidazolinylidenes and imidazolidines. *Tetrahedron* **1999,** *55*, 14523-14534.

52. Fischer, E. O.; Grubert, H., Über Aromatenkomplexe von Metallen. IV. Di-cyclopentadienyl-blei. *Z. Anorg. Allg. Chem.* **1956,** *286*, 237-242.

53. Fulmer, G. R.; Miller, A. J. M.; Sherden, N. H.; Gottlieb, H. E.; Nudelman, A.; Stoltz, B. M.; Bercaw, J. E.; Goldberg, K. I., NMR Chemical Shifts of Trace Impurities: Common Laboratory Solvents, Organics, and Gases in Deuterated Solvents Relevant to the Organometallic Chemist. *Organometallics* **2010,** *29*, 2176-2179.

54. Sheldrick, G., A short history of SHELX. *Acta Crystallogr. A* **2008,** *64*, 112-122.

55. Brand, R. A. *Normos. Mossbauer fitting Program*, Universitat Duisburg: Duisburg, Germany, 2002.

56. Becke, A. D., Density-functional thermochemistry. III. The role of exact exchange. *J. Chem. Phys.* **1993,** *98*, 5648-5652.

57. Lee, C.; Yang, W.; Parr, R. G., Development of the Colle-Salvetti correlation-energy formula into a functional of the electron density. *Phys. Rev. B* **1988,** *37*, 785-789.

58. Becke, A. D., Density-functional exchange-energy approximation with correct asymptotic behavior. *Phys. Rev. A* **1988,** *38*, 3098-3100.

59. Perdew, J. P., Density functional approximation for the correlation-energy of the inhomogeneous electron-gas. *Phys. Rev. B* **1986,** *33*, 8822-8824.

60. Grimme, S.; Antony, J.; Ehrlich, S.; Krieg, H., A consistent and accurate ab initio parametrization of density functional dispersion correction (DFT-D) for the 94 elements H-Pu. *J. Chem. Phys.* **2010,** *132*.

61. Grimme, S.; Ehrlich, S.; Goerigk, L., Effect of the Damping Function in Dispersion Corrected Density Functional Theory. *J. Comp. Chem.* **2011,** *32*, 1456-1465.

62. Weigend, F.; Ahlrichs, R., Balanced basis sets of split valence, triple zeta valence and quadruple zeta valence quality for H to Rn: Design and assessment of accuracy. *Phys. Chem. Chem. Phys.* **2005,** *7*, 3297-3305.

63. M. J. Frisch; G. W. Trucks; H. B. Schlegel; G. E. Scuseria; M. A. Robb; J. R. Cheeseman; G. Scalmani; V. Barone; B. Mennucci; G. A. Petersson; H. Nakatsuji; M. Caricato; X. Li; H. P. Hratchian; A. F. Izmaylov; J. Bloino; G. Zheng; J. L. Sonnenberg; M. Hada; M. Ehara; K. Toyota; R. Fukuda; J. Hasegawa; M. Ishida; T. Nakajima; Y. Honda; O. Kitao; H. Nakai; T. Vreven; J. A. Montgomery, J.; J. E. Peralta; F. Ogliaro; M. Bearpark; J. J. Heyd; E. Brothers; K. N. Kudin; V. N. Staroverov; R. Kobayashi; J. Normand; K. Raghavachari; A. Rendell; J. C. Burant; S. S. Iyengar; J. Tomasi; M. Cossi; N. Rega; J. M. Millam; M. Klene; J. E. Knox; J. B. Cross; V. Bakken; C. Adamo; J. Jaramillo; R. Gomperts; R. E. Stratmann; O. Yazyev; A. J. Austin; R. Cammi; C. Pomelli; J. W. Ochterski; R. L. Martin; K. Morokuma; V. G. Zakrzewski; G. A. Voth; P. Salvador; J. J. Dannenberg; S. Dapprich; A. D. Daniels; O. Farkas; J. B. Foresman; J. V. Ortiz; J. Cioslowski; D. J. Fox Gaussian 16, Revision A.03. Gaussian, Inc.: Wallingford CT, 2016.

64. Peng, C. Y.; Ayala, P. Y.; Schlegel, H. B.; Frisch, M. J., Using redundant internal coordinates to optimize equilibrium geometries and transition states. *J. Comp. Chem.* **1996,** *17*, 49-56.

65. McIver, J. W.; Komornic.A, Structure of Transition-state in organic reactions - General theory and an applications to cyclobutene-butadiene isomerization using a semiempirical molecular-orbital method. *J. Am. Chem. Soc.* **1972,** *94*, 2625-2633.

66. Atkins, P. W.; De Paula, J., *Physical Chemistry. 8th ed.*; Oxford: Oxford University Press: New York, 2006.

67. Wiberg, K. B., Application of People-Santry-Segal CNDO method to cyclopropylcarbinyl and cyclobutyl cation and to bicyclobutane. *Tetrahedron* **1968,** *24*, 1083-1096.

68. Reed, A. E.; Weinstock, R. B.; Weinhold, F., Natural-population analysis. *J. Chem. Phys.* **1985,** *83*, 735-746.

69. Reed, A. E.; Curtiss, L. A.; Weinhold, F., Intermolecular interactions from a natural bond orbital, donor-acceptor viewpoint. *Chem. Rev.* **1988,** *88*, 899-926.

70. Glendening, E. D.; Badenhoop, J. K.; Reed, A. E.; Carpenter, J. E.; Bohmann, J. A.; Morales, C. M.; Landis, C. R.; Weinhold, F. *GENNBO 6.0*, GENNBO 6.0; Theoretical Chemistry Institute, University of Wisconsin: Madison, WI, 2013.

71. Ziegler, T.; Rauk, A., Theoretical-study of the ethylene-metal bond in complexes between Cu^+, Ag^+, Au^+, Pt^0, or Pt^{2+} and ethylene, based on the Hartree-Fock Slater Transition-State method. *Inorg. Chem.* **1979,** *18*, 1558-1565.

72. Bickelhaupt, F. M.; Nibbering, N. M. M.; Van Wezenbeek, E. M.; Baerends, E. J., *J. Phys. Chem.* **1992,** *96*, 4864-4873.

73. te Velde, G.; Bickelhaupt, F. M.; Baerends, E. J.; Fonseca Guerra, C.; van Gisbergen, S. J. A.; Snijders, J. G.; Ziegler, T., Chemistry with ADF. *J. Comp. Chem.* **2001,** *22*, 931-967.

74. Krijn, J.; Baerends, E. J., *Fit Functions in the HFS-Method* **1984**.

75. Van Lenthe, E.; Baerends, E. J.; Snijders, J. G., *J. Chem. Phys.* **1993,** *99*, 4597-4610.

76. Hetzer, G.; Pulay, P.; Werner, H. J., Multipole approximation of distant pair energies in local MP2 calculations. *Chem. Phys. Lett.* **1998,** *290*, 143-149.

77. Pulay, P., Localizability of dynamic electron correlation. *Chem. Phys. Lett.* **1983,** *100*, 151-154.

78. Sæbø, S.; Pulay, P., Local configuration interaction: An efficient approach for larger molecules. *Chem. Phys. Lett.* **1985,** *113*, 13-18.

79. Hetzer, G.; Schütz, M.; Stoll, H.; Werner, H. J., Low-order scaling local correlation methods II: Splitting the Coulomb operator in linear scaling local second-order Møller-Plesset perturbation theory. *J. Chem. Phys.* **2000,** *113*, 9443-9455.

80. Saebø, S.; Pulay, P., Fourth-order Møller–Plessett perturbation theory in the local correlation treatment. I. Method. *J. Chem. Phys.* **1987,** *86*, 914-922.

81. Saebø, S.; Pulay, P., The local correlation treatment. II. Implementation and tests. *J. Chem. Phys.* **1988,** *88*, 1884-1890.

82. Schütz, M.; Hetzer, G.; Werner, H. J., Low-order scaling local electron correlation methods. I. Linear scaling local MP2. *J. Chem. Phys.* **1999,** *111*, 5691-5705.

83. Rauhut, G.; Pulay, P.; Werner, H. J., Integral transformation with low-order scaling for large local second-order Møller-Plesset calculations. *J. Comp. Chem.* **1998,** *19*, 1241-1254.

84. Pulay, P.; Saebø, S., Orbital-invariant formulation and second-order gradient evaluation in Møller-Plesset perturbation theory. *Theoretica Chimica Acta* **1986,** *69*, 357-368.

85. Werner, H.-J.; Knowles, P. J.; Knizia, G.; Manby, F. R.; Schütz, M.; Celani, P.; Korona, T.; Lindh, R.; Mitrushenkov, A.; Rauhut, G.; Shamasundar, K. R.; Adler, T. B.; Amos, R. D.; Bernhardsson, A.; Berning, A.; Cooper, D. L.; Deegan, M. J. O.; Dobbyn, A. J.; Eckert, F.; Goll, E.; Hampel, C.; Hesselmann, A.; Hetzer, G.; Hrenar, T.; Jansen, G.; Köppl, C.; Liu, Y.; Lloyd, A. W.; Mata, R. A.; May, A. J.; McNicholas, S. J.; Meyer, W.; Mura, M. E.; Nicklass, A.; O'Neill, D. P.; Palmieri, P.; Peng, D.; Pflüger, K.; Pitzer, R.; Reiher, M.; Shiozaki, T.; Stoll, H.; Stone, A. J.; Tarroni, R.; Thorsteinsson, T.; Wang, M. *MOLPRO, version 2012.1, a package of ab initio programs*: http://www.molpro.net., 2012.

86. Schütz, M.; Werner, H. J.; Lindh, R.; Manby, F. R., Analytical energy gradients for local second-order Moøller-Plesset perturbation theory using density fitting approximations. *J. Chem. Phys.* **2004,** *121*, 737-750.

87. Dunning Jr, T. H., Gaussian basis sets for use in correlated molecular calculations. I. The atoms boron through neon and hydrogen. *J. Chem. Phys.* **1989,** *90*, 1007-1023.

88. Woon, D. E.; Dunning Jr, T. H., Gaussian basis sets for use in correlated molecular calculations. III. The atoms aluminum through argon. *J. Chem. Phys.* **1993,** *98*, 1358-1371.

table of content graphic: